RSC Advances

PAPER

View Article Online
View Journal | View Issue

Cite this: *RSC Adv.*, 2025, **15**, 35068

One-step electrochemical aptasensor for lactate detection in athlete training using AuPt NPs and PEI-rGO composite with Na^+-dependent DNAzyme

Xu Han,[a] Haozhen Li *[b] and Ling Niu*[b]

This study introduces a novel electrochemical aptasensor designed for the sensitive detection of lactate in athlete sweat. The sensor is based on a PEI-rGO-modified SPCE coupled with AuPt NPs, and utilizes Na^+-assisted DNAzyme for signal amplification. The PEI-rGO modification enhances the aptasensor's conductivity, while the AuPt NPs efficiently load MB and LDNA, generating stable electrochemical signals. Furthermore, the Na^+-dependent DNAzyme leverages the Na^+ naturally present in sweat to activate the cleavage process, amplifying the detection signal. The sensor exhibits a strong linear relationship between current response and lactate concentration in the range of 5×10^{-3} to 10 mM, with a limit of detection (LOD) of 2.974 μM. It demonstrates excellent specificity, stability, and repeatability. The optimized aptasensor offers significant potential for real-time, non-invasive lactate monitoring, particularly in athletic performance and health assessment. This work provides a promising approach for the development of reliable, portable biosensors for tracking lactate metabolism, with implications for sports science and health management.

Received 16th June 2025
Accepted 3rd September 2025

DOI: 10.1039/d5ra04257g

rsc.li/rsc-advances

1 Introduction

Lactate is a glycolytic metabolic product produced during physiological muscle activity in low-oxygen environments and serves as an important biomarker reflecting metabolic status.[1] In particular, during exercise, lactate metabolism can effectively reflect an athlete's training performance, helping to optimize subsequent training strategies.[2] However, invasive methods for directly measuring lactate levels in muscles have high requirements, which not only make it difficult to assess an athlete's physical condition in real-time but also carry the risk of infection.[3] Human sweat contains abundant metabolic substances, including lactate, and its concentration changes according to the body's exercise state.[4] Under resting conditions, the lactate concentration in human sweat is around 0.5–1 mM, whereas during intense exercise, it can rise to 5–20 mM.[5] While the human body can metabolize lactate into pyruvate through the liver under healthy conditions,[6] excessive lactate accumulation or sustained concentrations at moderate to high levels (≥5 mM) can lead to issues such as tissue perfusion deficits, lactate acidosis, and other symptoms. Excessive lactate in the body can also cause health problems like hemorrhage, respiratory failure, ischemia, and kidney issues.[7] Therefore, it is crucial to be able to quickly, reliably, and non-invasively monitor lactate metabolism in athletes during training.

Considering the need for accurate detection of trace lactate in sweat, methods such as high-performance liquid chromatography (HPLC) and gas chromatography-mass spectrometry (GC-MS) can indeed provide precise and reliable data.[8,9] However, these techniques require expensive and bulky instruments, complex operating procedures, and skilled personnel. Therefore, they are not suitable for quickly and conveniently obtaining real-time data during an athlete's training. Immunochromatography and colorimetric methods are often considered attractive alternatives due to their low cost, portability, and fast processing time, which have garnered attention from professionals in relevant fields.[10,11] However, these methods have lower sensitivity and insufficient specificity, making them inadequate for reliable detection. In contrast, electrochemical detection technology is known for its fast response, strong specificity, miniaturized equipment, and flexible operation in the sensing field. Therefore, combining this novel detection technology offers a feasible approach for rapidly and reliably measuring lactate levels in athletes.

So far, various electrochemical strategies have been developed for detecting lactate in sweat. Many of these approaches rely on enzyme recognition and catalysis, such as lactate oxidase (LOx) and lactate dehydrogenase (LDH).[12,13] Undoubtedly, the high catalytic efficiency and fast response of enzymes are promising. However, enzymes are highly sensitive to environmental pH and temperature, which presents potential challenges in practical detection processes.[14] Additionally, these enzymes are often sourced from different types of bacteria, meaning there may be slight variations in enzyme activity and

[a]*Department of Sports, Beijing Institute of Graphic Communication, Beijing, China*
[b]*Department of Physical Education, Zhengzhou University(Main Campus), Zhengzhou, China. E-mail: lihaozhen01@zzu.edu.cn*

optimal conditions, which could affect the stability of the detection sensor.[15] Therefore, employing nucleic acids to construct sensing platforms offers a promising strategy. Although nucleic acid probes may be less robust under extreme conditions—such as high temperatures, or strong ionic environments—they also possess unique advantages compared to protein-based enzymes in many biosensing applications. Specifically, nucleic acids offer greater programmability and chemical modifiability, enabling more precise control over signal transduction. Moreover, nucleic acids are free from batch-to-batch variability, which contributes to higher detection accuracy and reproducibility.[16] Taken together, while the limitations of nucleic acids should not be overlooked, their advantages render them highly attractive components in the development of flexible and reliable biosensing strategies.[16] DNA-based dynamic circuits can be designed to convert target molecular information into a nucleic acid response signal upon input.[17] It is important to note that aptamers (Apt) play a key role as the signal conversion elements in DNA dynamic circuits. Aptamers, which are short single-stranded DNA or RNA oligonucleotides, can specifically bind to target molecules through their conformational properties and are generated through the *in vitro* selection process of exponential enrichment ligand systems (SELEX).[18] Thus, in the construction of detection sensors, aptamers can effectively perform the task of specific recognition of target molecules.

Moreover, introducing DNAzymes into DNA dynamic circuits can enhance the sensitivity of the sensor.[19] Unlike natural proteases, DNAzymes are metal ion-dependent artificial enzymes, possessing excellent stability and tunable enzymatic activity. This means the cleavage ability of DNAzymes is controllable. The conditions determining the cleavage ability of DNAzymes include the presence of metal ions that activate their enzymatic activity and DNA substrates modified with RNA base sites. Multiple metal ions can activate responsive DNAzymes, such as Pb^{2+},[20] Cu^{2+},[21] Mg^{2+},[22] and Na^{+}.[23] Considering that Na^{+} is a metal ion abundantly present in sweat,[24] utilizing Na^{+}-dependent DNAzymes to construct DNA network circuits for signal amplification is a highly effective approach. By utilizing the Na^{+} naturally present in sweat to activate DNAzyme, the construction cost can be reduced, and it can also serve as an initial safeguard to ensure the detection sensor operates in the environment where sweat is produced on the skin.

In this work, we developed a DNA dynamic circuit based on lactate-specific aptamers (Apt) and Na^{+}-driven DNAzyme, coupled with AuPt nanoparticles loaded with methylene blue (MB) as a signal tag, to enable rapid and sensitive detection of lactate levels in sweat during athlete training. Specifically, Na^{+}-driven DNAzyme sequences and the well-prepared MB@AuPt NPs signal tags were functionalized onto the surface of flexible screen-printed carbon electrodes (SPCE) using nucleic acid sequences, creating a portable biosensing electrode. When sweat is secreted onto the skin surface, it connects the biosensor's detection region. Lactate and Na^{+} sequentially activate the designed DNA dynamic circuit, leading to the DNAzyme-mediated cleavage of the signal tag, which in turn releases the signal and ultimately results in a decreased electrochemical response. This nucleic acid-based strategy, relying on electrochemical signal output, offers a convenient and effective approach for wearable electrochemical biosensors and provides a competitive concept for lactate detection.

2 Experimental section

2.1 Chemicals and apparatus

Reduced graphene oxide [(rGO), Shanghai Macklin Biochemical Company, 99.9%], sodium chloride (NaCl, Shanghai Aladdin Reagent Company, 99.5%), lactate (LA, Shanghai Macklin Biochemical Company, 99.9%), glucose (Shanghai Aladdin Reagent Company, 98.0%), urea (Shanghai Aladdin Reagent Company, 99.0%), acetic acid (Shanghai Aladdin Reagent Company, 99.8%), 6-mercapto-1-hexanol (MCH, Shanghai Yuan Ye Bio-Technology Co., Ltd, Shanghai, China), chloroplatinic acid (H_2PtCl_6, Shanghai Yuan Ye Bio-Technology Co., Ltd, Shanghai, China), methylene blue (MB, Shanghai Yuan Ye Bio-Technology Co., Ltd, Shanghai, China), chloroauric acid ($HAuCl_4$, Sangon Biotech Co., Ltd, Shanghai, China), L-ascorbic acid (AA, Xilong Chemical Co., Ltd, Guangdong, China), polyethyleneimine (PEI, Xilong Chemical Co., Ltd, Guangdong, China), diethylene glycol (DEG, Shanghai Yuan Ye Bio-Technology Co., Ltd, Shanghai, China). All oligonucleotide sequences employed in this study were synthesized by Sangon Biotech (Shanghai, China), artificial sweat (YuanYe Bio-Technology Co., Ltd, China). The detailed sequences are provided below:

Apt: 5′– CTC TCG ACG ACG AGT AGC GCG TAT GAA TGC TTT TCT ATG GAG TCG TC – 3′;

Label-DNA (LDNA): 5′–NH_2–TTT TTT TTT TCG ATC TCC TAT/rA/GGA AGT TCC GCC – 3′;

DNAzyme: 5′– COOH–TTT TTT TTT TTT TTT TTT TTT TTT GA CGA CTC CAT AGA GAC TGA TGT TGA GGC GGA ACC AGG TCA AAG GTG GGT GAG GGG ACG CCA AGA GTC CCC GCG GTT AGG AGA TCG GCT ACT CGT CGT GAG – 3′.

Electrochemical measurements were performed using a CHI660E electrochemical workstation (Shanghai Chenhua Instrument, China) equipped with a standard three-electrode system. Material characterization was performed using a variety of instruments, including a transmission electron microscope (TEM, HT7700, Hitachi, Japan), scanning electron microscope (SEM, Quanta Feg 250, Japan), Fourier transform infrared spectrometer (FTIR, Nicolet 6700, Bruker, Germany).

2.2 Synthesis of PEI-rGO

To prepare PEI-rGO, 0.5 grams of polyethyleneimine (PEI) were completely dissolved in 50 milliliters of deionized water. Then, 100 milligrams of rGO powder was added and dispersed under ultrasonic treatment. The resulting PEI-rGO solution was refluxed at 100 °C for 12 hours under nitrogen protection. After the reaction, the black solid was separated by centrifugation and washed five times with deionized water to remove excess PEI. Finally, the obtained PEI-rGO product was dried in a vacuum oven at 80 °C for 12 hours until fully dry.

2.3 Synthesis of AuPt NPs

The synthesis of Au nanoparticles (Au NPs) was carried out using a modified polyol reduction method, as described in the literature.[25] Initially, 0.18 g of PVP K30 and 0.073 g of CTAB were added to 20 mL of DEG solution, which was stirred for 30 min until dissolved. The solution was then heated in an oil bath at 195 °C for 10 min, resulting in solution A. Next, 0.032 g of CTAB and 200 μL of a 0.1 M $HAuCl_4 \cdot 3H_2O$ aqueous solution were mixed with 2 mL of DEG solution. After 5 min of magnetic stirring to ensure uniform mixing, solution B was obtained. Solution B was added to solution A, and the mixture was reacted at 210 °C for 40 minutes. After the reaction, the product was separated by centrifugation, washed with water, and finally dispersed in 1 mL of ultrapure water.

The synthesis method for AuPt NPs followed a similar procedure as for Au NPs. First, 0.18 g of PVP K30 and 0.073 g of CTAB were dissolved in 20 mL of DEG solution and stirred for 30 min. The solution was then heated at 195 °C in an oil bath for 10 min to obtain solution A. Next, 70 μL of a 0.1 g mL^{-1} $HAuCl_4 \cdot 3H_2O$ aqueous solution and 200 μL of a 0.1 M $H_2PtCl_6 \cdot 6H_2O$ aqueous solution were mixed, and this mixture was added to 2 mL of DEG solution containing 0.032 g of CTAB. After 5 min of stirring, solution B was obtained. Finally, solution A and solution B were mixed and reacted at 210 °C for 40 minutes. After the reaction, the product was separated by centrifugation, washed, and dispersed in 1 mL of ultrapure water.

2.4 Synthesis of the AuPt NPs/LDNA/MB hybrids probe

First, 100 μL of AuPt NPs and 100 μL of LDNA (5 μM) were incubated at 37 °C for 12 hours in a shaking incubator to obtain AuPt NPs/LDNA. Unbound LDNA was removed by centrifugation. The resulting product (AuPt NPs/LDNA) was then dispersed in 200 μL of methylene blue (MB) solution and incubated at 37 °C for 12 hours in a shaking incubator. Unbound MB was removed by centrifugation. Finally, 2 μL of 1% BSA was added, and the mixture was shaken to obtain AuPt NPs/LDNA/MB. The final product (AuPt NPs/LDNA/MB) was dispersed in 400 μL of Tris–HCl buffer (pH 7.4) and stored for subsequent use.

2.5 Synthesis of the Apt/DNAzyme duplex

To prepare the Apt/DNAzyme duplex, 50 μL of DNAzyme (4 μM) and 50 μL of Apt (4 μM) were mixed and heated at 95 °C for 5 minutes. The mixture was then slowly cooled to room temperature to obtain the Apt/DNAzyme duplex.

2.6 Fabrication of the sensing electrode

Before use, the SPCE should be pretreated following these steps. First, immerse the working area of the SPCE completely in a 0.5 M H_2SO_4 solution and perform cyclic voltammetry within the potential range of −1.0 to +1.0 V until a relatively stable electrochemical signal is obtaine.[26] After completion, rinse the treated SPCE with ultrapure water and store it for later use. 5 μL of the prepared PEI-rGO solution was dropped onto the working area of the SPCE. The electrode was then left to air dry at room temperature for subsequent use. Then, the AuPt NPs/LDNA/MB hybrid probe and Apt/DNAzyme duplex were modified onto the working area of the SPCE surface at a 1 : 12 concentration ratio (10 μL). After incubating for 2 hours, the surface was washed with Tris buffer to remove any excess unreacted materials. The resulting electrode was then immersed in a 2 mM MCH solution for 1 h to block the non-specific adsorption effects, facilitating the formation of a well-aligned DNA monolayer. The electrode was stored in buffer solution at 4 °C before use.

3 Results and discussion

3.1 Principle of the electrochemical aptasensor

The detection principle of the constructed electrochemical aptamer sensor is described in detail in Scheme 1. The detection method consists of three main components: the PEI-rGO functionalized nanomaterials that modify the sensor interface, the Apt for specific recognition of the target, and the DNAzyme for signal amplification. Specifically, PEI-rGO, AuPt NPs/LDNA/MB, and the Apt/DNAzyme duplex are sequentially modified onto the sensor working interface, awaiting activation by the target analyte. After the sweat permeates the aptasensor, the electrode interface is provided with an adequate solution system, and the three-electrode setup is connected to trigger the detection strategy. Lactate in the sweat can specifically bind to the Apt, causing the Apt to release and expose the active sequence of the Na^+-dependent DNAzyme. Meanwhile, the abundant Na^+ in the sweat can spontaneously activate the DNAzyme's cleavage activity. At this point, the DNAzyme freely cleaves the surrounding AuPt NPs/LDNA/MB signal tags because the LDNA has been pre-modified with recognition sites (rA) that can be cleaved by the DNAzyme. Continuous cleavage causes the signal tags to move away from the aptasensor surface, resulting in a decrease in the electrochemical signal. Experimental observations and analysis show that the presence of LA significantly affects the electrochemical response, and the response is positively correlated with the concentration of the target analyte.

3.2 Characterization of the nanomaterials

As shown in Fig. 1A, the morphology of the prepared PEI-rGO nanomaterials was characterized by TEM. The PEI-rGO exhibits a large and relatively flat two-dimensional sheet-like structure, providing a larger specific surface area for the sensor surface. To confirm the successful functionalization of rGO, FTIR was used to analyze both rGO and PEI-rGO. As seen in the FTIR results in Fig. 1B, the peaks at 1605 cm^{-1}, 1582 cm^{-1}, and 1065 cm^{-1} correspond to the C=C, –OH, and C–O epoxy stretching vibrations, respectively, which are characteristic peaks of rGO. In the PEI-rGO spectrum, the characteristic peaks of rGO disappear, and a new peak appears at 2924 cm^{-1}, which can be attributed to the $-CH_2$ stretching vibration on the PEI chain, confirming the successful preparation of PEI-rGO.[26]

In Fig. 1C, the TEM image shows the overall morphology of the prepared AuPt NPs. The AuPt NPs are spherical with

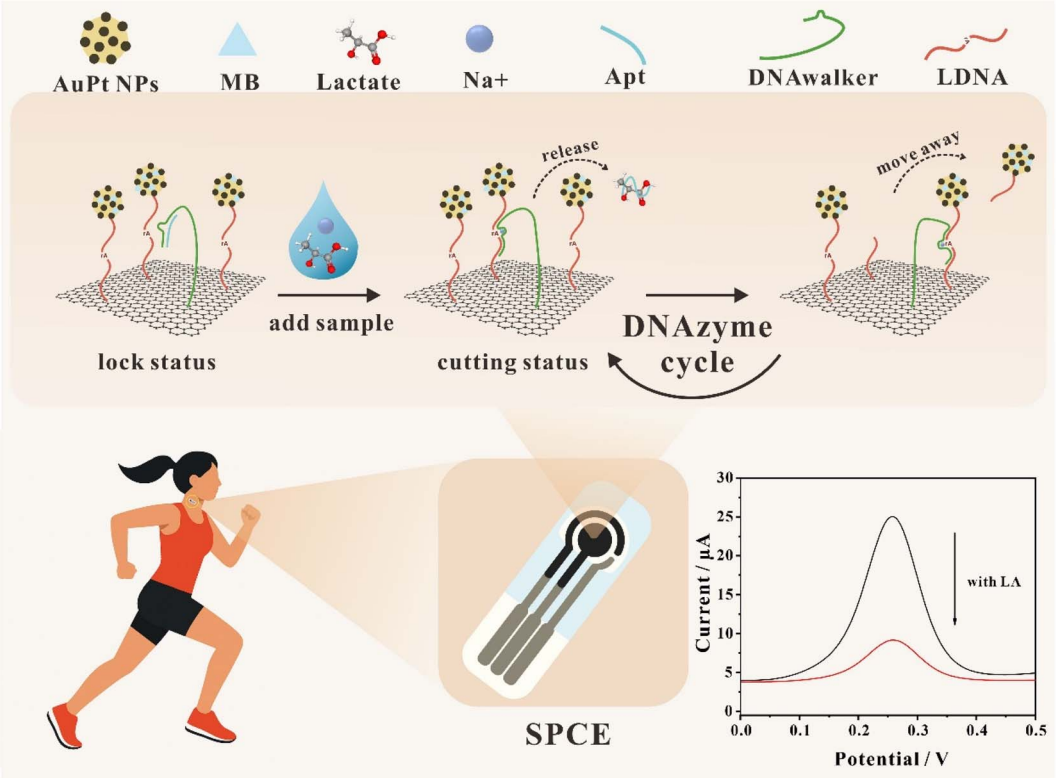

Scheme 1 Illustration of the aptasensor based on PEI-rGO and Na^+-dependent DNAzyme for sensitive detection of lactate (LA) in athlete sweat.

a diameter of approximately 80 nm, and their surface is covered with dense small-sized particles. Fig. 1D presents the HRTEM of AuPt NPs, offering a clearer view of the material details. Elemental mapping analysis (Fig. 1E and F) provides information on the distribution of Au and Pt elements in the prepared AuPt NPs. It is clearly observed that the Au element is more concentrated in the center, while the Pt element is more distributed in the outer layer, presenting a core-shell-like distribution. Moreover, the distribution of each element is uniform, confirming the successful preparation of AuPt NPs.

3.3 Characterization of the aptasensor

The stepwise modification process of the aptamer sensor was systematically analyzed using Electrochemical Impedance Spectroscopy (EIS), as depicted in Fig. 2A. Curve a represents the impedance of the bare SPCE, exhibiting a small semicircular arc. Upon modification of the SPCE with PEI-rGO (curve b), a decrease in impedance was observed, which can be attributed to the successful functionalization of PEI-rGO. The enhanced conductivity of PEI-rGO facilitates improved electron transfer rates, leading to reduced impedance. Subsequently, the signal labels AuPt NPs/LDNA/MB were introduced onto the electrode surface (curve c). The immobilization of the signal labels caused a slight increase in the radius of the semicircular arc, which can be explained by the spatial hindrance resulting from the attachment of the signal tags. Although AuPt NPs exhibit excellent conductivity, the negatively charged phosphate backbone of LDNA impedes efficient electron transfer, contributing to the observed increase in impedance. Following this, the Apt/DNAzyme duplex was immobilized onto the aptasensor surface (curve d), further increasing the impedance, as indicated by the larger semicircle radius. Curve e corresponds to the incubation of MCH on the aptasensor surface, which serves to block non-specific binding sites. Due to the non-conductive nature of MCH, the impedance increases further, as reflected in the larger radius of the semicircle. The gradual monitoring of these steps through EIS clearly demonstrates the successful fabrication of the aptasensor.

After the construction of the aptasensor, it is essential to verify the feasibility of its detection strategy. As shown in Fig. 3A, the cyclic voltammetry (CV) current responses of the bare SPCE and the PEI-rGO-modified SPCE are compared. A clear observation is made that the PEI-rGO-modified SPCE generates a significantly larger current response. This can be attributed to the enhanced electron transfer efficiency at the aptasensor interface provided by the PEI-rGO modification. To further validate this, differential pulse voltammetry (DPV) was employed to detect the current response generated by the signal label (Fig. 3B). The DPV current response is also noticeably increased ($\Delta I = 1.872$ μA), supporting the conclusion that PEI-rGO modification effectively enhances the electron transfer and detection capability of the aptasensor. In Fig. 3C, in the absence of the target, the aptasensor exhibits a higher DPV signal response because the Na^+-dependent DNAzyme remains inactive and cannot cleave the signal label AuPt NPs/LDNA/MB. As a result, more conductive electrons generated by methylene

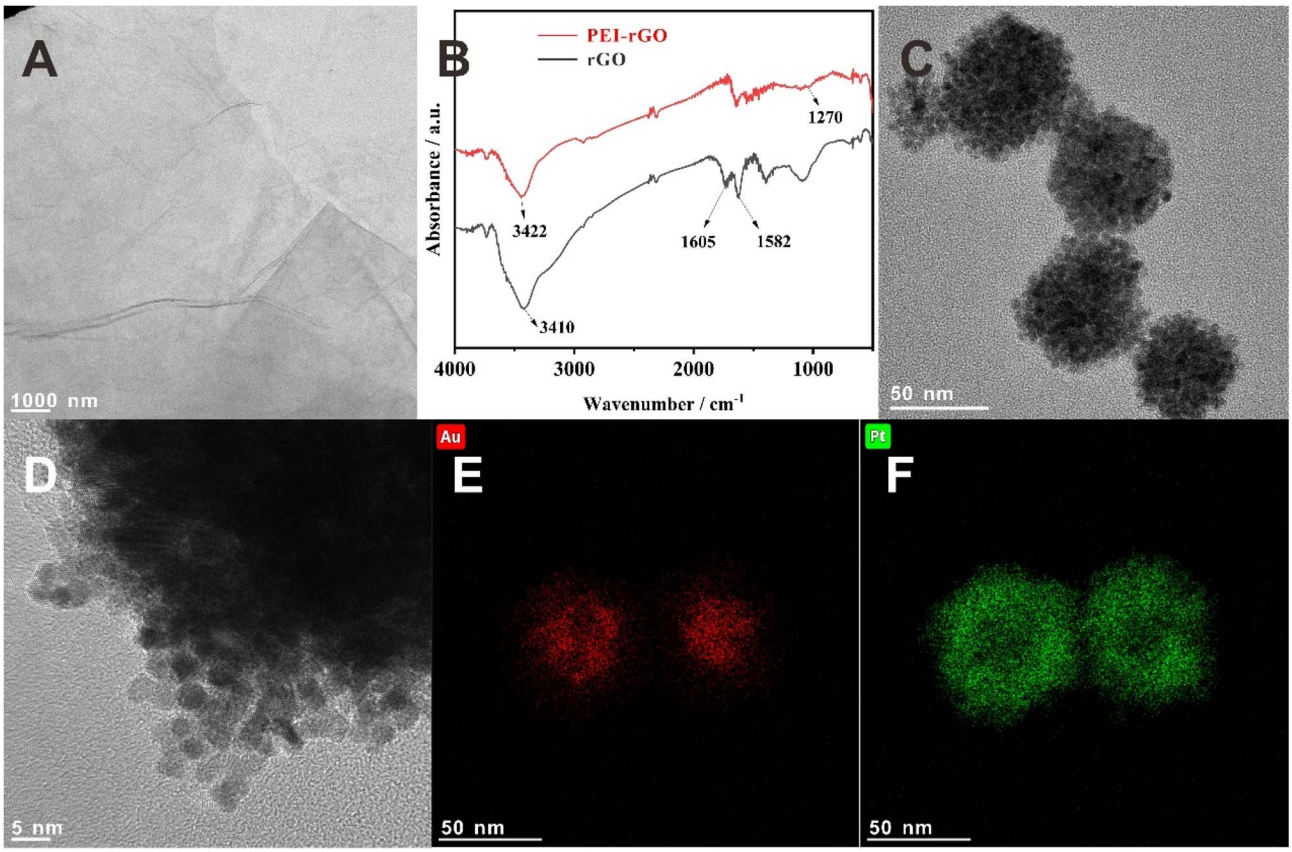

Fig. 1 (A) TEM images of PEI-rGO, (B) FTIR images of rGO (black) and PEI-rGO (red); (C) TEM images of AuPt NPs, (D) HRTEM images of AuPt NPs, (E and F) elemental mapping images of Au and Pt images of AuPt NP.

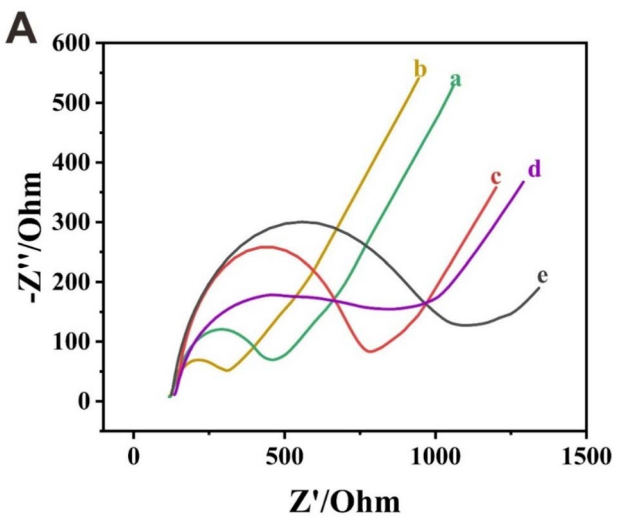

Fig. 2 (A) EIS of (a) bare SPCE, (b) SPCE/PEI-rGO, (c) SPCE/PEI-rGO/AuPt NPs/LDNA/MB, (d) SPCE/PEI-rGO/AuPt NPs/LDNA/MB/Apt/DNAzyme duplex, (e) SPCE/PEI-rGO/AuPt NPs/LDNA/MB/Apt/DNAzyme duplex/MCH was performed in 5 mM $[Fe(CN)_6]^{3-/4-}$.

blue (MB) are detectable at the electrode surface. However, when the simulated sweat sample containing the target LA and Na^+ was introduced into the detection system, a significant decrease in the DPV current was observed. This indicates that the target LA has bound to the Apt, releasing the active cleavage sequence of the DNAzyme, which, in the presence of Na^+, activates the cleavage of the surrounding signal labels AuPt NPs/LDNA/MB. The continuous cleavage process causes the signal tags to move away from the electrode surface, leading to a significant reduction in the signal. In addition, the importance of Na^+ in the detection system requires further confirmation. Therefore, a validation experiment was designed to address this. Two conditions were tested: one where Na^+ was introduced into the system, and another where Na^+ was absent, with both conditions containing the target LA. As shown in Fig. 3D, a clear difference in DPV responses was observed between the two conditions. This can be attributed to the fact that even if the DNAzyme possesses the cleavage sequence, without the presence of Na^+, no cleavage events can occur. In conclusion, the strategy designed in this work is indeed feasible and effective.

3.4 Optimization of experimental conditions

We explored the influence of three factors—namely, the concentration of PEI-rGO nanomaterials used for modifying the aptasensor interface, the ratio of Apt/DNAzyme duplex to AuPt NPs/LDNA/MB, and the incubation time of lactate—on the current response of the aptasensor. The primary objective was

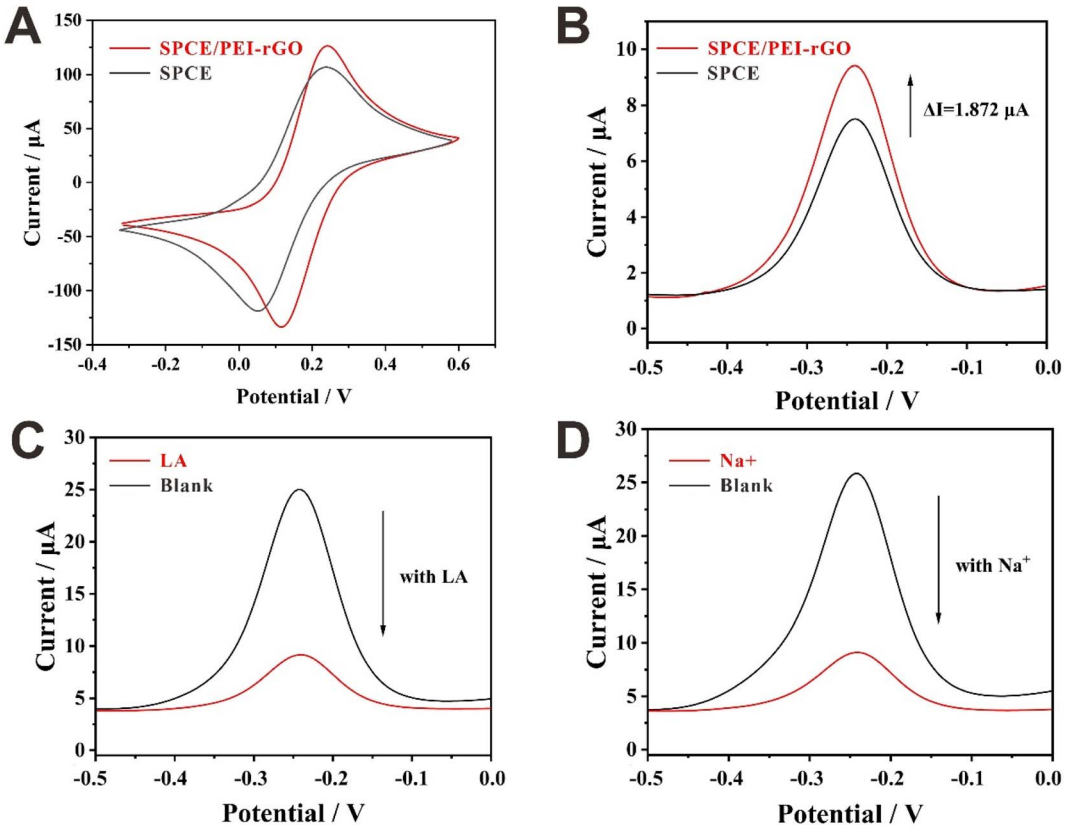

Fig. 3 (A) CV of different modified electrodes: bare SPCE (black curve), SPCE/PEI-rGO (red curve); (B) DPV of different modified electrodes: bare SPCE (black curve), SPCE/PEI-rGO (red curve); (C) DPV of the electrode under different conditions: in the presence of target LA (red curve), in the absence of target LA (black curve); (D) DPV of the electrode under different conditions: in the presence of Na^+ (red curve), in the absence of Na^+ (black curve).

to further optimize the aptasensor's capacity for target detection. Each factor was examined independently to assess its individual impact on the current response, thereby facilitating the identification of the optimal conditions for enhanced aptasensor performance. In Fig. 4A, as the PEI-rGO concentration increases from 0.5 μM to 2.5 μM, the DPV response first rises and then slightly decreases. This indicates that PEI-rGO enhances the conductivity of SPCE, but the subsequent decrease in current may be due to an excessively high concentration of PEI-rGO, which leads to the accumulation of surplus nanomaterials, thereby hindering electron transfer efficiency. The ratio of DNAzyme to the cutting substrate is another crucial factor influencing the detection performance of the aptasensor, as it directly impacts the cleavage efficiency. In Fig. 4B, when the ratio of Apt/DNAzyme duplex to AuPt NPs/LDNA/MB reaches 1 : 12, the current response peaks. Further increasing the ratio to

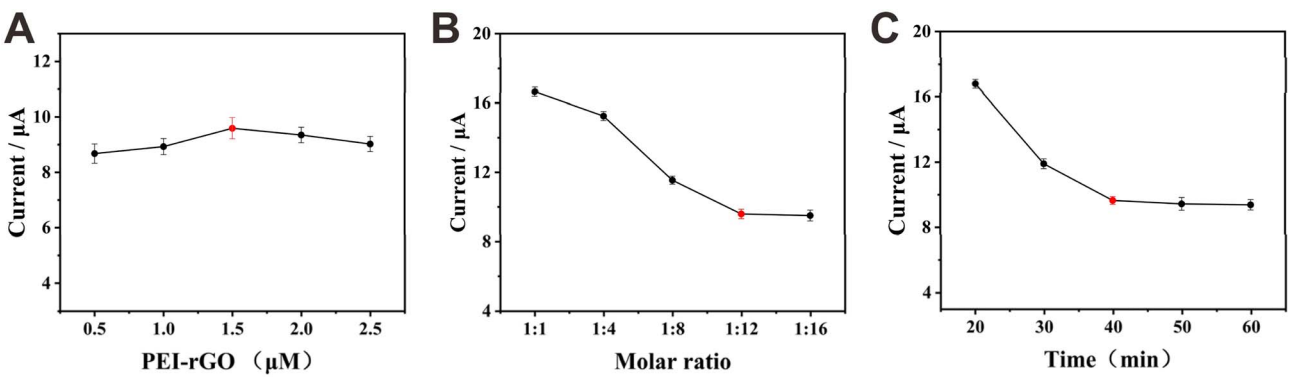

Fig. 4 Optimization of the (A) concentration of PEI-rGO, (B) molar ratio of Apt/DNAzyme duplex and AuPt NPs/LDNA/MB, (C) incubation time of LA. Error bar = SD ($n = 3$).

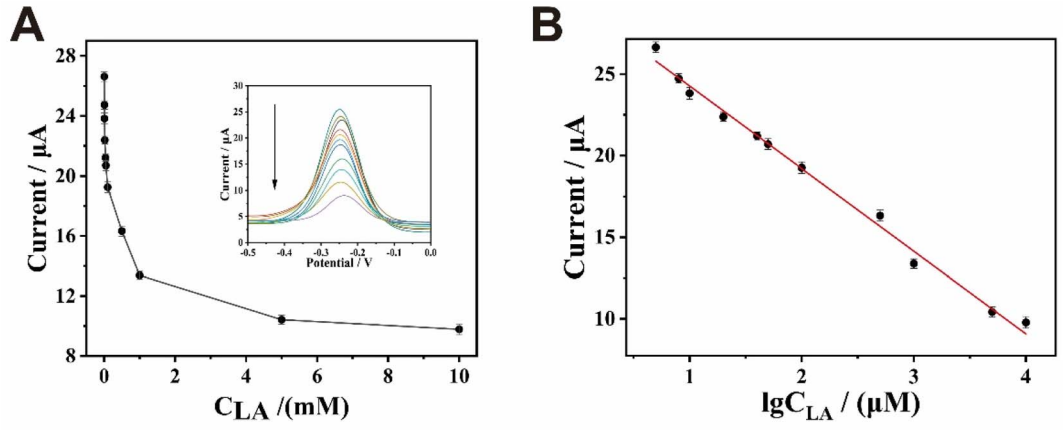

Fig. 5 (A) Response of the aptasensor to different concentrations of lactate (5×10^{-3} to 10 mM). (B) The linear relationship between DPV intensity and lactate concentration in an exponential range.

1 : 16 does not result in an additional increase in current, suggesting that the cleavage efficiency of the DNAzyme has reached saturation at a ratio of 1 : 12. Fig. 4C demonstrates the effect of lactate incubation time on the aptasensor's detection performance. It can be observed that the DPV current increases with time and stabilizes after 40 minutes. The results show that the current value saturates at a lactate incubation time of 40 minutes, and subsequent experiments were performed with a 40-minute incubation time.

3.5 Analytical performance of the aptasensor

Under the optimal experimental conditions, we evaluated the detection performance of the aptasensor designed in this study. As shown in Fig. 5A, within the concentration range of 5×10^{-3} to 10 mM (5 μM, 8 μM, 10 μM, 20 μM, 40 μM, 50 μM, 100 μM, 500 μM, 1 mM, 5 mM, 10 mM), the DPV response gradually decreased as the lactate concentration increased. Fig. 5B demonstrates a linear relationship between the DPV signal response and lactate concentration within the 5×10^{-3} to 10 mM range, with the linear equation given by $I = -5.07 \lg C_{LA} + 2.93$. The LOD was found to be 2.974 μM, with a correlation coefficient (R^2) of 0.99.

Furthermore, considering that the aptasensor was designed for the detection of lactate concentration in sweat, it is essential to evaluate whether other components in sweat could interfere with the detection performance of the aptasensor. To evaluate the specificity of the aptasensor, we selected representative potential interferents commonly found in human sweat, including glucose (5 mM), urea (100 mM), chloride ions (Cl^-, 100 mM), glutamic acid (1 mM), and aspartic acid (1 mM). The concentrations used were deliberately set higher than their maximum reported physiological levels in sweat.[27] As shown in Fig. 6A, under the presence of other interfering substances, the aptasensor's response closely matches the current response generated in the blank experiment. A noticeable decrease in current response was only observed in the presence of lactate. When all interfering substances were mixed with the target lactate and tested, the current response still decreased, with results similar to those obtained with lactate alone. This demonstrates that the designed aptasensor exhibits excellent interference resistance. Stability and repeatability are also crucial parameters for evaluating the detection performance of the aptasensor. As shown in Fig. 6B, the aptasensors from the same batch retained approximately 87% of their initial current

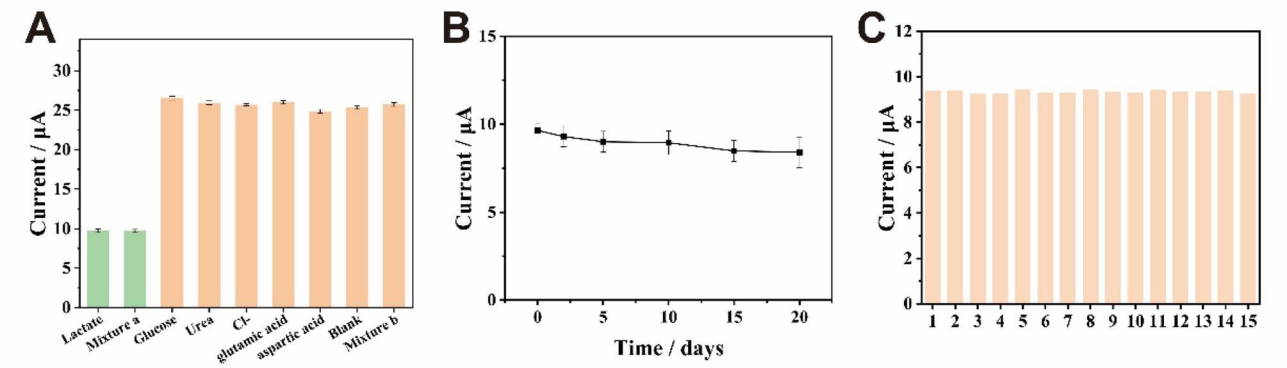

Fig. 6 (A) Specificity of the aptasensor (mixture a: with lactate; mixture b: without lactate); (B) long-term stability testing of the aptasensor; (C) repeatability of the aptasensor.

Table 1 Detection of lactate in real samples

Sample	Added (μM)	Found (μM)	Recovery (%)	RSD (%, $n = 3$)
1	0.1	0.098	98%	4.13%
2	0.1	0.11	101%	5.01%
3	1	0.92	92%	3.7%
4	1	0.97	97%	4.8%
5	5	4.75	95%	2.35%
6	5	4.91	98.2%	3.11%

response after 20 days of storage, indicating satisfactory stability within an acceptable range for practical applications. As shown in Fig. 6C, a total of 15 electrodes from the same fabrication batch were tested under consistent experimental conditions. The current responses were highly consistent across all samples, and the calculated relative standard deviation (RSD) was as low as 0.66%, demonstrating the excellent reproducibility of the aptasensor. In summary, the aptasensor designed in this study demonstrates excellent interference resistance, stability, and repeatability.

3.6 Real samples analysis

After confirming the excellent detection performance of the designed aptasensor, we applied it to real sample testing to evaluate its ability to detect lactate concentrations in actual sweat samples. Different concentrations of lactate were added to artificial sweat (lactate-free), with the specific results shown in Table 1.

The results revealed that the recovery rate ranged from 92% to 101%, and the relative standard deviation (RSD) ranged from 2.35% to 5.01%. These results demonstrate the promising application prospects of this platform for the quantitative detection of lactate in sweat.

4 Conclusion

This work demonstrates an aptasensor based on PEI-rGO-modified SPCE combined with AuPt NPs nanomaterials, utilizing Na^+-assisted DNAzyme for signal amplification to detect lactate in athlete sweat. Specifically, PEI-rGO provides an optimal detection microenvironment for the aptasensor. AuPt NPs efficiently load MB and LDNA, stably generating electrochemical signals, while Na^+-assisted DNAzyme utilizes Na^+ present in sweat as an activation agent to amplify the signal through cyclic processes. During the lactate detection process, a good linear relationship was observed between the current response and the logarithm of lactate concentration in the range of 5×10^{-3} to 10 mM, demonstrating excellent specificity, stability, and repeatability. This work highlights the significant potential of this aptasensor for monitoring lactate levels in human sweat, offering valuable insights for tracking athlete health status and training conditions.

Conflicts of interest

We declare that we do not have any commercial or associative interest that represents a conflict of interest in connection with the work submitted.

Data availability

All data supporting this study are included in the article.

References

1 Y. Zhao, M. Li, X. Yao, Y. Fei, Z. Lin, Z. Li, K. Cai, Y. Zhao and Z. Luo, HCAR1/MCT1 Regulates Tumor Ferroptosis through the Lactate-Mediated AMPK-SCD1 Activity and Its Therapeutic Implications, *Cell Rep.*, 2020, **33**, 108487, DOI: 10.1016/j.celrep.2020.108487.

2 B. S. Ferguson, M. J. Rogatzki, M. L. Goodwin, D. A. Kane, Z. Rightmire and L. B. Gladden, Lactate metabolism: historical context, prior misinterpretations, and current understanding, *Eur. J. Appl. Physiol.*, 2018, **118**, 691–728, DOI: 10.1007/s00421-017-3795-6.

3 T. Jiang, Y.-F. Ji and T.-C. Ma, Development of a photoelectrochemical blood lactate sensor for athletes, *Alex. Eng. J.*, 2025, **121**, 370–378, DOI: 10.1016/j.aej.2025.02.103.

4 F. Alam, S. RoyChoudhury, A. H. Jalal, Y. Umasankar, S. Forouzanfar, N. Akter, S. Bhansali and N. Pala, Lactate biosensing: The emerging point-of-care and personal health monitoring, *Biosens. Bioelectron.*, 2018, **117**, 818–829, DOI: 10.1016/j.bios.2018.06.054.

5 D. Jiang, C. Xu, Q. Zhang, Y. Ye, Y. Cai, K. Li, Y. Li, X. Huang and Y. Wang, In-situ preparation of lactate-sensing membrane for the noninvasive and wearable analysis of sweat, *Biosens. Bioelectron.*, 2022, **210**, 114303, DOI: 10.1016/j.bios.2022.114303.

6 A. E. Jones and M. A. Puskarich, Sepsis-Induced Tissue Hypoperfusion, *Crit. Care Clin.*, 2009, **25**, 769–779, DOI: 10.1016/j.ccc.2009.06.003.

7 P. J. Derbyshire, H. Barr, F. Davis and S. P. J. Higson, Lactate in human sweat: a critical review of research to the present day, *J. Physiol. Sci.*, 2012, **62**, 429–440, DOI: 10.1007/s12576-012-0213-z.

8 C.-L. Hsieh, R. Koga, A. Furusho, T. Akita, M. Mita, T. Ide, J.-A. Lee and K. Hamase, Enantioselective and simultaneous determination of lactate and 3-hydroxybutyrate in human plasma and urine using a narrow-bore online two-dimensional high-performance liquid chromatography system, *J. Sep. Sci.*, 2018, **41**, 1298–1306, DOI: 10.1002/jssc.201701283.

9 M. Numako, T. Toyo'oka, I. Noge, Y. Kitagawa, H. Mizuno and K. Todoroki, Risk assessment of diabetes mellitus using dried saliva spot followed by ultra-performance liquid chromatography with fluorescence and mass spectrometry, *Microchem. J.*, 2018, **142**, 202–207, DOI: 10.1016/j.microc.2018.06.037.

10 A. J. Lakade, K. Sundar and P. H. Shetty, Nanomaterial-based sensor for the detection of milk spoilage, *LWT*, 2017, **75**, 702–709, DOI: **10.1016/j.lwt.2016.10.031**.

11 Z. Ran, X. Wang, L. Zhang, Y. Yang, Z. Shang, Q. Chen, X. Ma, Z. Qian and W. Liu, Enzymatic colorimetric method for turn-on determination of l-lactic acid through indicator displacement assay, *J. Biosci. Bioeng.*, 2023, **136**, 159–165, DOI: **10.1016/j.jbiosc.2023.06.001**.

12 P. Bollella, S. Sharma, A. E. G. Cass and R. Antiochia, Microneedle-based biosensor for minimally-invasive lactate detection, *Biosens. Bioelectron.*, 2019, **123**, 152–159, DOI: **10.1016/j.bios.2018.08.010**.

13 F. Alam, S. RoyChoudhury, A. H. Jalal, Y. Umasankar, S. Forouzanfar, N. Akter, S. Bhansali and N. Pala, Lactate biosensing: The emerging point-of-care and personal health monitoring, *Biosens. Bioelectron.*, 2018, **117**, 818–829, DOI: **10.1016/j.bios.2018.06.054**.

14 Y. Liu and X. Xu, An electrochemical aptasensor for the detection of bisphenol A based on triple signal amplification assisted by gold nanoparticles, hemin/G-quadruplex DNAzyme, and exonuclease I, *Microchim. Acta*, 2025, **192**, 25, DOI: **10.1007/s00604-024-06882-4**.

15 G. Liu, C. Ho, N. Slappey, Z. Zhou, S. E. Snelgrove, M. Brown, A. Grabinski, X. Guo, Y. Chen, K. Miller, J. Edwards and T. Kaya, A wearable conductivity sensor for wireless real-time sweat monitoring, *Sens. Actuators, B*, 2016, **227**, 35–42, DOI: **10.1016/j.snb.2015.12.034**.

16 A. D. Ellington and J. W. Szostak, In vitro selection of RNA molecules that bind specific ligands, *Nature*, 1990, **346**, 818–822, DOI: **10.1038/346818a0**.

17 X. Ni, B. Xia, L. Wang, J. Ye, G. Du, H. Feng, X. Zhou, T. Zhang and W. Wang, Fluorescent aptasensor for 17β-estradiol determination based on gold nanoparticles quenching the fluorescence of Rhodamine B, *Anal. Biochem.*, 2017, **523**, 17–23, DOI: **10.1016/j.ab.2017.01.021**.

18 M. Darmostuk, S. Rimpelova, H. Gbelcova and T. Ruml, Current approaches in SELEX: An update to aptamer selection technology, *Biotechnol. Adv.*, 2015, **33**, 1141–1161, DOI: **10.1016/j.biotechadv.2015.02.008**.

19 E. Osman, S. Saxena, S. Qian, J. L'Heureux-Hache, P. Li, J. Manek, J. Gu, T. Hoare, Y. Li and L. Soleymani, Electrochemical detection of Legionella pneumophila using DNAzymes and under continuous flow in cooling tower water, *Biosens. Bioelectron.*, 2025, **278**, 117283, DOI: **10.1016/j.bios.2025.117283**.

20 C. B. Swearingen, D. P. Wernette, D. M. Cropek, Y. Lu, J. V. Sweedler and P. W. Bohn, Immobilization of a Catalytic DNA Molecular Beacon on Au for Pb(II) Detection, *Anal. Chem.*, 2005, **77**, 442–448, DOI: **10.1021/ac0401016**.

21 Y. Takezawa, H. Zhang, K. Mori, L. Hu and M. Shionoya, Ligase-mediated synthesis of CuII-responsive allosteric DNAzyme with bifacial 5-carboxyuracil nucleobases, *Chem. Sci.*, 2024, **15**, 2365–2370, DOI: **10.1039/D3SC05042D**.

22 B.-F. Yuan, Y. Xue, M. Luo, Y.-H. Hao and Z. Tan, Two DNAzymes targeting the telomerase mRNA with large difference in Mg^{2+} concentration for maximal catalytic activity, *Int. J. Biochem. Cell Biol.*, 2007, **39**, 1119–1129, DOI: **10.1016/j.biocel.2007.03.004**.

23 S.-F. Torabi and Y. Lu, Identification of the Same Na+-Specific DNAzyme Motif from Two *In Vitro* Selections Under Different Conditions, *J. Mol. Evol.*, 2015, **81**, 225–234, DOI: **10.1007/s00239-015-9715-7**.

24 S.-F. Torabi, P. Wu, C. E. McGhee, L. Chen, K. Hwang, N. Zheng, J. Cheng and Y. Lu, *In vitro* selection of a sodium-specific DNAzyme and its application in intracellular sensing, *Proc. Natl. Acad. Sci. U. S. A.*, 2015, **112**, 5903–5908, DOI: **10.1073/pnas.1420361112**.

25 H. Liu, W. Zheng, Y. Zhao and Y. Zhou, Plasmon-Enhanced Electroactivity of AuRu Nanostructures for Electroanalysis Applications, *Anal. Chem.*, 2021, **93**, 4944–4951, DOI: **10.1021/acs.analchem.0c05439**.

26 J. Fu, X. An, Y. Yao, Y. Guo and X. Sun, Electrochemical aptasensor based on one step co-electrodeposition of aptamer and GO-CuNPs nanocomposite for organophosphorus pesticide detection, *Sens. Actuators, B*, 2019, **287**, 503–509, DOI: **10.1016/j.snb.2019.02.057**.

27 X. Weng, M. Li, L. Chen, B. Peng and H. Jiang, A wearable nanozyme–enzyme electrochemical biosensor for sweat lactate monitoring, *Talanta*, 2024, **279**, 126675, DOI: **10.1016/j.talanta.2024.126675**.